Higher order mode excitations in gyro-amplifiers*

K. T. Nguyen,[†,a)] J. P. Calame, B. G. Danly, B. Levush, M. Garven,[b)] and T. Antonsen, Jr.[c)]
Vacuum Electronics Branch, Naval Research Laboratory, Washington, DC 20375

(Received 26 October 2000; accepted 8 December 2000)

In gyro-devices, a nonlinear output taper is often employed as the transition from the near cutoff radius of the interaction circuit to a much larger output waveguide. The tapers are usually designed to avoid passive mode conversion, and thus do not consider the effect of a bunched beam. However, recent simulations with the self-consistent MAGY code [Botton *et al.*, IEEE Trans. Plasma Sci. **26**, 882 (1998)] indicate that higher order mode interactions with the bunched electron beam can substantially compromise the mode purity of the rf output. The interaction in the taper region is traveling wave in nature, and is strongly dependent on the residual beam bunching characteristics resulting from the upstream operating mode interaction. An experiment has been performed to quantify the rf output mode content from a *Ka*-band gyroklystron. The agreement between salient theoretical and measured rf output characteristics confirms the existence of higher order mode excitation in output tapers as predicted by theory. © *2001 American Institute of Physics.*
[DOI: 10.1063/1.1348330]

I. INTRODUCTION

A key element in the design of gyro-amplifier rf structures is the minimization of unwanted mode excitations. High mode purity is critical in order to minimize undesirable rf absorption and reflection in the ensuing transmission line. Also, for radar applications, the presence of spurious modes can result in unnecessary sidelobes of radiated pulses and inadequate duplexer performance. Thus, good rf matching with high modal purity across the operating band is an integral part of the component design process. Consequently, it is a key consideration in the design of output uptapers, which are employed in gyro-devices to serve as the transition from the near cutoff dimensions of the interaction circuit to a larger dimension waveguide.[1] This transition may be necessitated by thermal considerations of spent-beam collectors or by requirements dictated by the size of output windows.

Irrespective of the taper types (i.e., discrete, linear, or nonlinear), the profile of the output taper is carefully shaped in order to minimize mode conversion in cold test and to achieve the required radial transition in a reasonable distance.[2,3] In the past, the beam–wave interaction was not a major concern in the taper design process. Recently, a theoretical study with the quasi-three-dimensional code MAGY[4] shows that the presence of the bunched electron beam can alter the delicate balance intended by the original design and substantially compromises the mode purity of the outgoing rf.[5] This effect is most pronounced in the regime where the bunched electron beam is still energetic upon entering the uptaper, such as the low drive power portion of the drive curve or the edges of the bandwidth curve.[5] These observations motivate an experiment at the Naval Research Laboratory to further investigate the impact of this phenomenon.

This experiment, to measure the modal content of the rf output from a four-cavity *Ka*-band gyroklystron,[6] has recently been completed. Good agreement between theoretical prediction and experimental data in terms of the output rf mode content strongly suggests that beam–wave interaction in the taper can play a major role in spoiling the intended rf output mode purity. This paper presents the results from the experimental measurement, the data analysis, and the comparison with theory. The organization of the remainder of the paper is as follows. Section II provides the theoretical basis for the phenomena. Section III describes the experiment and data analysis. Section IV presents the comparison between theory and experimental data. Section V presents conclusions and suggests possible solutions to reduce the spurious mode content.

II. THEORETICAL DESCRIPTION

All uptapers are carefully designed in order to minimize mode conversion within a reasonable length. A commonly employed uptaper geometric profile is the Dolph–Chebyshev profile due to its superior mode purity within a short length.[2,3] Figure 1 illustrates such a Dolph–Chebyshev nonlinear uptaper. The particular uptaper shown was employed as the transition from the radius of the TE_{01} output cavity to the beam collector radius in the *Ka*-band gyroklystrons.[6–8] The radial transition from a radius of approximately 0.55 cm to a radius of 1.90 cm occurs over an axial length of 7.3 cm. The mode conversion/reconversion characteristics of this uptaper are also illustrated in Fig. 1. Shown are the power profiles for the TE_{01} and the total rf power as a function of axial length, as well as the axial power profile of the dominant higher order mode, TE_{02}, from a MAGY simulation.[4]

*Paper VI3 2, Bull. Am. Phys. Soc. **45**, 294 (2000).
[†]Invited speaker.
[a)]Also at KN Research, Silver Spring, MD 20905.
[b)]Also at Omega-P., Inc., New Haven, CT 06520.
[c)]Also at University of Maryland, College Park, MD 20742.

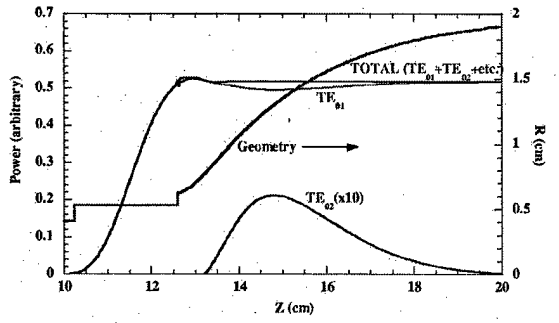

FIG. 1. Output cavity and taper geometry of the four-cavity Ka-band TE_{01} gyroklystron. Also shown are the axial power profiles from the MAGY simulation in the absence of beam. Note that the power profile for the TE_{02} mode has been multiplied by a factor of 10.

Note that the power profile for the TE_{02} mode has been multiplied by a factor of 10 for better illustration.

The power profile shown in Fig. 1 has been obtained in the absence of the electron beam. The cavity has been excited with a TE_{01} current source with a Gaussian axial profile[5] and the simulation includes five different modes (TE_{01}, TE_{02},..., and TE_{05}). It can be readily noted that in the absence of the electron beam the rf power in the operating mode (TE_{01}) is first converted to higher order modes before being reconverted back to the operating mode. This can clearly be seen by observing that the TE_{01} mode dips as the TE_{02} peaks, while the total rf power remains constant. For this particular design, the content of the dominant higher order mode (TE_{02}) peaks at around 4% inside the uptaper. Of course, the level of the higher order mode content inside the uptaper is strongly dependent on the actual geometry. As an additional illustration, Fig. 2 shows the geometry and the decomposition of the rf power into various modes as a function of axial distance for the Dolph–Chebyshev uptaper employed in the TE_{01} W-band gyroklystron without the electron beam.[5,9] It can be readily seen from Fig. 2 that the higher order mode content temporarily exceeds 20% inside the uptaper. Even with such a high peak level of higher order modes, mode purity is better than -37 dB at the end of the uptaper.

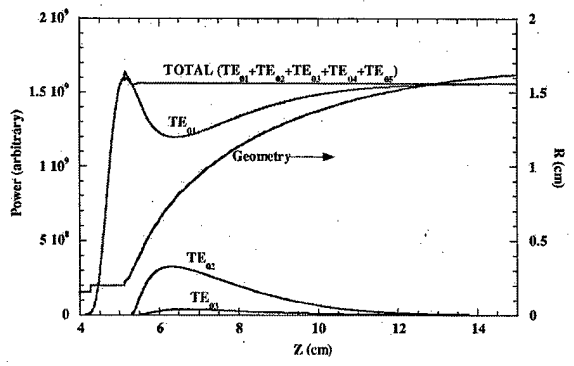

FIG. 2. Output cavity and taper geometry of a W-band TE_{01} gyroklystron. Also shown are the axial power profiles from the MAGY simulation in the absence of beam (Ref. 4).

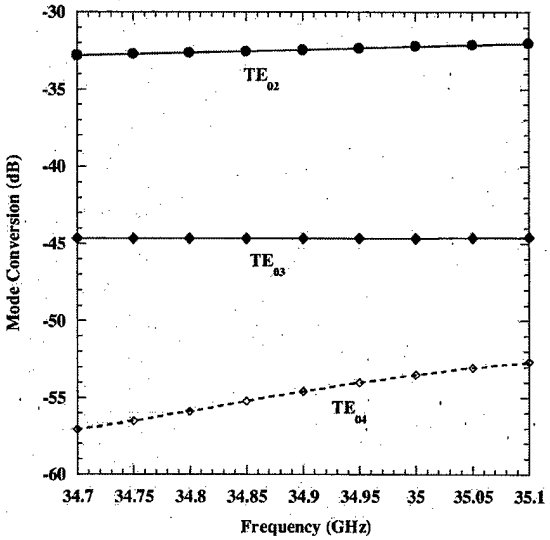

FIG. 3. Higher order mode contents at the end of output taper shown in Fig. 1.

For the Ka-band uptaper, the final higher order content across the frequency band of interest in the absence of the electron beam is as shown in Fig. 3. Thus, with a well-designed uptaper, the mode purity can be quite high across the band in the absence of the electron beam. This level of mode purity is strongly dependent on the delicate process of up and down mode conversion as the rf power flows downstream through the uptaper, as shown in previous figures. However, it was found that beam-wave interaction in the uptaper can substantially perturb this delicate process, which can cause a substantial degradation of the mode purity across the band.

The perturbation in the presence of the electron beam can be understood as follows. As the electron beam and the rf power exit the main interaction region and enter the uptaper, the rf power undergoes a conversion to higher order modes as described in the previous paragraph. The presence of rf power in higher order modes is one of the two key ingredients involved in the perturbation. The other is the resonance condition required for beam–wave interaction in the higher order modes. This resonance condition for any particular mode is met approximately at the intersection of the Doppler shifted beam line,

$$\omega = \Omega_c(z) + k_{zn}(z) v_z, \tag{1}$$

and the waveguide dispersion curve of the mode,

$$\omega^2 = \omega_{cn}(z)^2 + k_{zn}(z)^2 c^2. \tag{2}$$

In the above equation, ω is the operating angular frequency, Ω_c is the electron cyclotron frequency, ω_{cn} and k_{zn} are the angular cutoff frequency and the axial wave number of the TE_{0n} mode, respectively. Once the resonance condition is met for any particular mode, the rf power present in that mode as a result of the uptaper internal mode conversion can interact with the electron beam. It is this interaction that perturbs the delicate balance of rf power flow intended by the cold design.

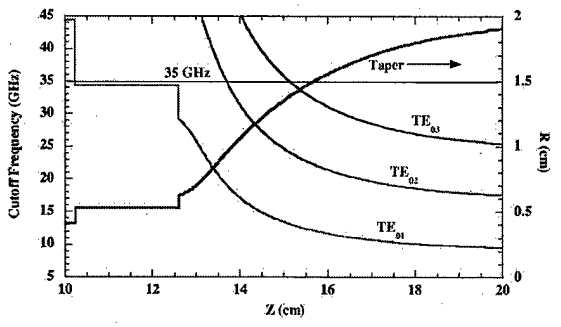

FIG. 4. Geometry and cutoff frequency for various modes of the taper shown in Fig. 1.

The interaction is that of the gyro-traveling-wave type. The uptaper interaction is expected to be stronger when the interaction with the operating mode in the main circuit is weaker. Thus, the perturbation is most pronounced at low rf output power and it is at a minimum at saturation. Also, since the radius of the uptaper is rapidly changing, the cutoff frequency is also a rapid function of axial distance. This is illustrated in Fig. 4, which shows the cutoff frequency for various modes as a function of axial distance for the Ka-band uptaper. Consequently, the resonance condition can only be satisfied over a short distance. Moreover, it is expected that the interaction strength of the higher order mode beam–wave interaction in the uptaper is also sensitive to the magnetic field profile, as can be seen from Eqs. (1) and (2).

The effect of beam–wave interaction on mode conversion in the uptaper is illustrated by Fig. 5, which shows the axial power profile for the TE_{01}, TE_{02}, TE_{03}, and total rf power from a MAGY simulation. Figure 5 can be compared with Fig. 1, which shows the rf power profiles without the beam. The substantial change in the axial power profile for the higher order modes in Fig. 5 represents the effect of beam–wave interaction in the uptaper. A comparison with Fig. 1 shows the significant degradation of the mode purity. It is these observations that motivated the experiment described in Sec. III.

III. EXPERIMENT

A diagram of the experiment is shown in Fig. 6. The axis-symmetric output radiation from the four-cavity gyroklystron amplifier[6] passes through an output window and is

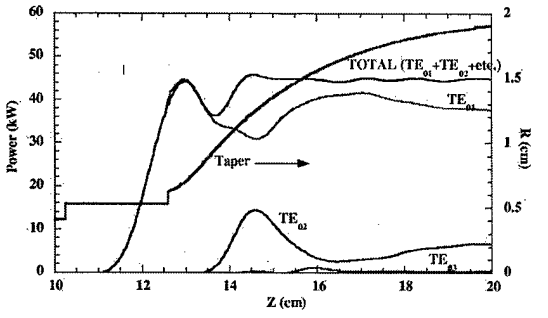

FIG. 5. Geometry and axial power profiles from a MAGY simulation for taper shown in Fig. 1 in the presence of an electron beam.

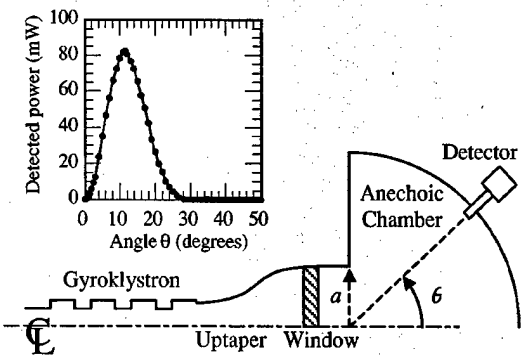

FIG. 6. Diagram of the experimental setup. The inset is a measured radiation pattern of the detector power vs polar angle θ at the nominal gyroklystron operating point.

launched into an anechoic chamber. The circular launching aperture of the chamber, with radius $a=1.90\,\text{cm}$, lies on a metal ground plane that covers one side of the chamber. The remaining surfaces are covered with cones of lossy microwave absorbing material. A portion of the radiated power is collected by a short length of Ka-band waveguide that protrudes into the chamber. The collected power passes through a calibrated chain of attenuators and is measured with an HP8990A peak power analyzer. The chamber is designed to allow the pickup antenna to sweep in polar angle θ relative to the central axis of the experiment, while maintaining a constant radius of 76.52 cm relative to the center of the radiating aperture. This arrangement permits the measurement of a radiation pattern, such as the example shown in the inset plot of Fig. 6.

The radiation pattern in Fig. 6 was obtained at a nominal operating point that produced 190 kW of saturated output power in 2 μs pulses at 34.90 GHz, with a gain of 49 dB and an efficiency of 30.1%. The beam voltage, current, and velocity ratio were 70.2 kV, 9 A, and 1.33, respectively, and the circuit magnetic field was 13.07 kG. The same radiation pattern is plotted on a logarithmic power scale in Fig. 7 (triangles). The plotted power is normalized to the peak value of the single large lobe, which occurs at 11.5°. The

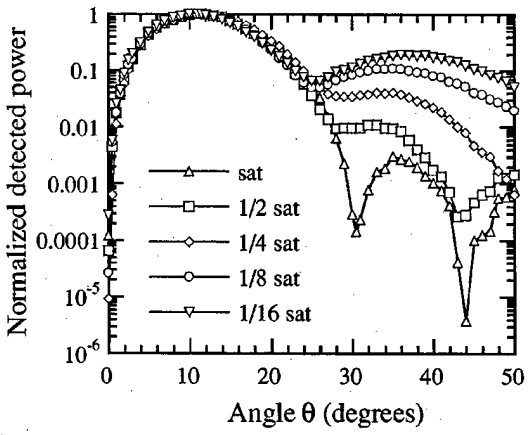

FIG. 7. Measured radiation patterns at 34.9 GHz at various fractions of saturated output power. Each curve has been normalized to its maximum value.

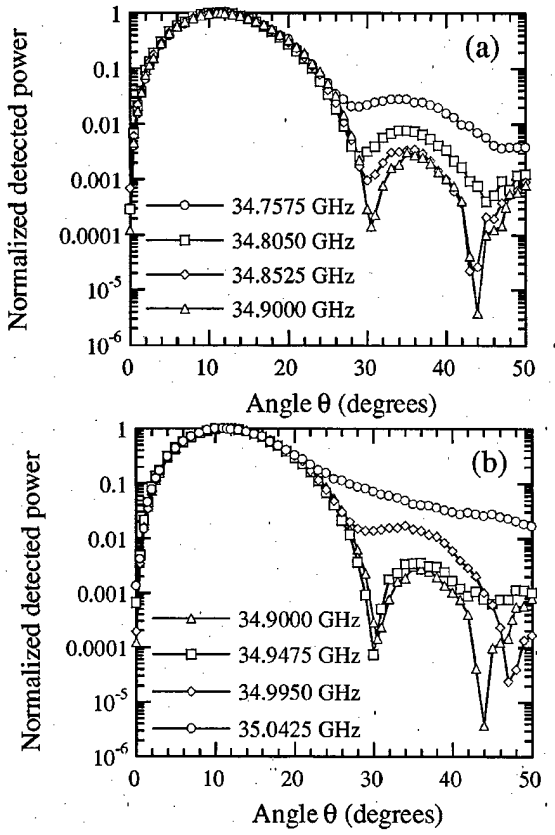

FIG. 8. Measured radiation patterns at various drive frequencies below (a) and above (b) the center frequency. Each curve has been normalized to its maximum value, and used a drive power of 2.4 W.

single large lobe and the deep minima near 30° and 44° are consistent with a nearly pure TE_{01} mode, as expected at saturation. To explore the effect of reduced output power on modal purity, a series of radiation patterns were measured at output powers corresponding to 1/2, 1/4, 1/8, and 1/16 of the saturated output power at the nominal operating point. The reduced output powers were obtained by reducing the input power by the appropriate amount, while all other operating parameters were unchanged, including the 34.90 GHz drive frequency. The measured radiation patterns, each normalized to their respective maximum values, are also plotted in Fig. 7. The degradation in modal purity with decreasing output power is visible first as a filling-in of the minima, followed by the formation of a substantial secondary lobe near 38°.

A second series of measurements studied the variation of modal purity with drive frequency. Radiation pattern measurements were obtained at three frequencies below the center frequency, as shown in Fig. 8(a), and three frequencies above the center frequency, as shown in Fig. 8(b). The behavior at the center frequency is replotted in each part of Fig. 8 for clarity. In all cases the drive power was held constant at 2.4 W, which was the level required to saturate the amplifier at 34.90 GHz. Within the 3 dB total bandwidth of the gyroklystron (±110 MHz), only a modest filling-in of the minima occurs, but significant impurities appear at larger frequency offsets. The effect is more pronounced on the high frequency side.

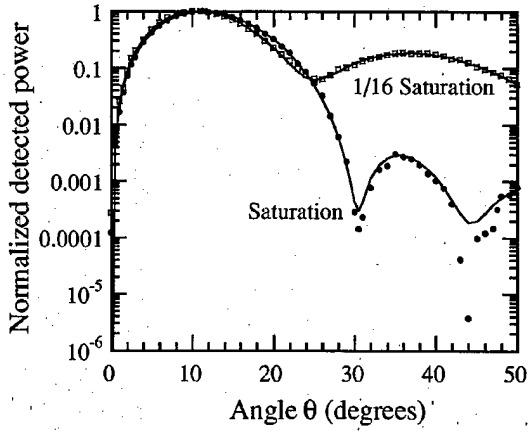

FIG. 9. Comparisons between the measured radiation pattern data (symbols) and the results of the far-field curve fitting procedure, for saturated output power and 1/16 of saturated output power conditions.

A curve-fitting procedure was employed to convert the radiation patterns into quantitative measurements of modal purity. The electric field at the detector location can be accurately represented by a sum of the far-field radiation patterns,[10] each created by pure TE_{0m} modes at the aperture. These individual electric far fields are of the form

$$E_m(\theta)=\cos\theta\frac{J_1(ka\sin\theta)}{x_{0m}'^2-(ka\sin\theta)^2}, \tag{3}$$

where k is the free space wave number and x_{0m}' are the Bessel roots for TE modes. The expression for the detected power P due to all modes is given by

$$P(\theta)=2\left|\sum_{m=1}^{M} C_m E_m(\theta)\Big/\int_0^{\pi/2}\sin\theta E_m^2(\theta)d\theta\right|^2, \tag{4}$$

where C_m is a complex amplitude of the TE_{0m} mode. The power in the mth mode, p_m, expressed as a fraction of the total power, is given by

$$p_m=|C_m|^2\Big/\left(\sum_{i=1}^{M}|C_i|^2\right). \tag{5}$$

To create the curve fit, an objective function was defined as the sum of the squares of the differences between the observed power at each data angle and the computed value at that angle [given by Eq. (4)]. A weighting function of the form $1+w_f\tan^2\theta\sin\theta$ was used to emphasize the fitting at large angles, which is where the higher order modes have the most impact. A typical value for the weighting factor w_f was 50, although 150 had to be used on occasion. The fitting procedure was initialized by assuming a pure TE_{01} mode, which provides a rough value for C_1. Following this, the values of the real and imaginary parts of C_m were updated in a sequential, steepest-descent coordinate search, until no further improvement of the objective function was obtained. Examples of curve fits are shown in Fig. 9, for the saturated nominal operating point and for the point at 1/16 saturation. The specific numeric values for the modal contents will be presented later in the paper.

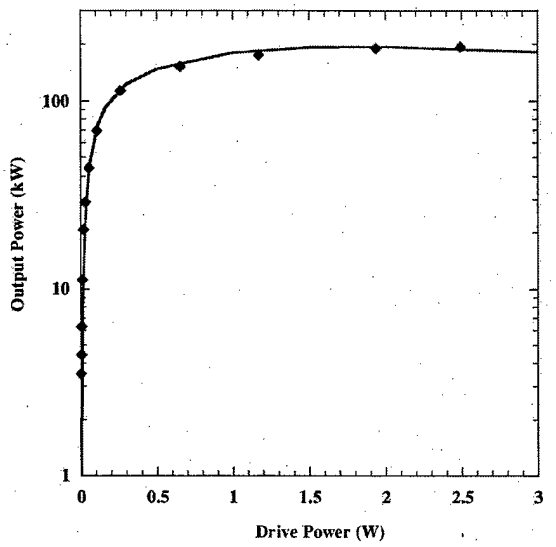

FIG. 10. Drive curve of the four-cavity Ka-band gyroklystron at the center frequency of 34.90 GHz with a 70.2 kV, 6 A, α=1.33, electron beam. Solid line and symbols are MAGY results and experimental data, respectively.

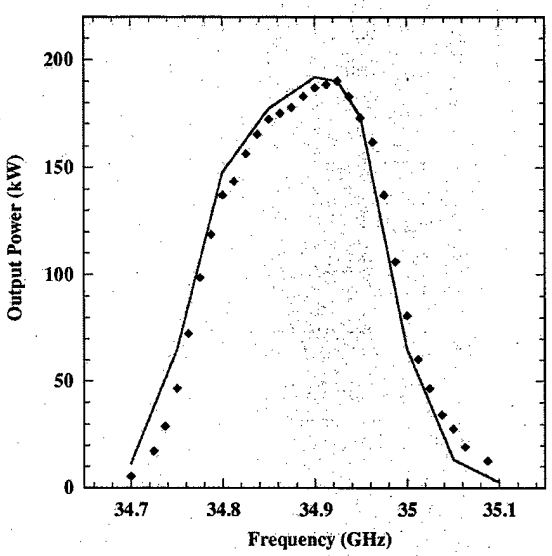

FIG. 11. Saturated bandwidth of the four-cavity Ka-band gyroklystron at drive power of 2.4 W with a 70.2 kV, 6 A, α=1.33, electron beam. The solid line and symbols are MAGY results and experimental data, respectively.

Finally, it is important to quantify the effects of measurement error on the computed modal contents. To accomplish this, the measured power data points were randomly perturbed by up to $\pm 3\%$, and an additional, additive random error in the detected power level of up to ± 5 μW was simultaneously imposed. Top-hat distributions were used in both perturbations. When the perturbed data set is subjected to curve fitting, a slightly different modal content results, and by repeating the procedure 1000 times a most probable set of modal contents was obtained for each radiation pattern. Error bounds were simultaneously obtained.

IV. SIMULATION AND EXPERIMENTAL DATA COMPARISON

In order to verify that the experimentally observed behavior described in Sec. III is indeed due to beam–wave interaction in the uptaper, we have performed simulations with MAGY for direct comparison with experimental data. MAGY has previously been successfully used to model both W-band and Ka-band gyroklystrons.[5–8] It has also been used for designing a gyro-traveling-wave-tube.[11] In particular, it was used to model the four-cavity Ka-band gyroklystron used in the present experiment.[6]

Using known experimental parameters as input, we simulated the drive curve and bandwidth curve for comparing against experimental data. Shown in Fig. 10 is the drive curve of the gyroklystron. The agreement between simulation (solid line) and experimental data (dots) is good. Similar agreement is also obtained for the saturated bandwidth curve, which is plotted in Fig. 11. As mentioned, this good agreement has been obtained by using known experimental parameters as input to the simulations. These parameters include beam current, voltage, velocity ratio, cavity resonance frequencies and quality factors, and magnetic field profile. The only assumption is the beam velocity spread, which is taken to be 5.5% based on EGUN simulations.[12]

The good agreement between simulation and experiment in terms of the drive and bandwidth curves provides the necessary confidence that the simulation model is accurate at least up to the output cavity. This is important since the interaction inside the uptaper is heavily dependent on the beam bunching characteristics and the rf power resulting from the beam–wave interaction in the main circuit region (the four cavities) in addition to the correct magnetic field profile.

The modal content as a fraction of the outgoing rf power plotted as a function of the drive power is shown in Fig. 12 at the center frequency of 34.90 GHz. This curve is similar to Fig. 10 except the fractional mode contents are being shown

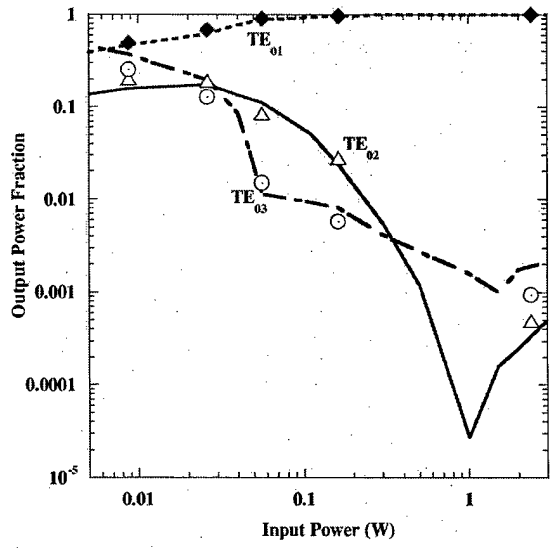

FIG. 12. Modal contents as a function of drive power for the drive curve shown in Fig. 10. The line and symbols are MAGY results and experimental data, respectively.

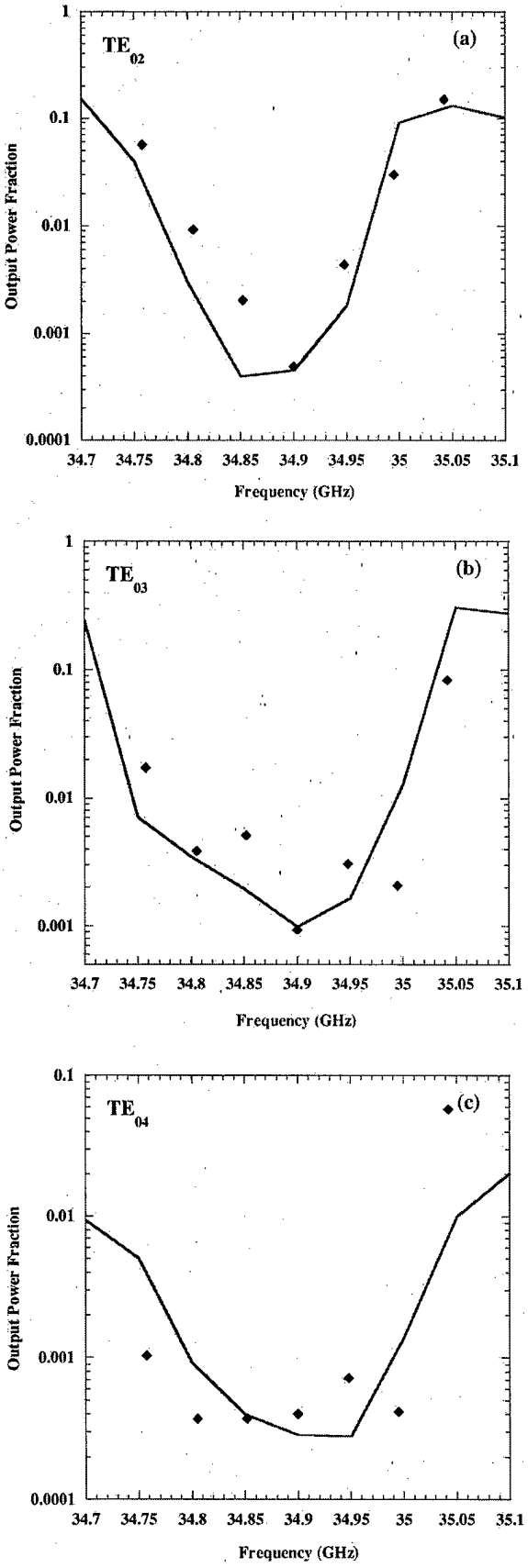

FIG. 13. Modal contents as a function of frequency corresponding to the bandwidth curve shown in Fig. 11. From top to bottom, the modes are TE_{01}, TE_{03}, and TE_{04}. The line and symbols are MAGY results and experimental data, respectively.

for the vertical axis. The simulation results and experimental data are shown as solid lines and symbols, respectively, in the figure for TE_{01}, TE_{02}, and TE_{03} modes. Note that the experimental data points were obtained using the data analysis technique described in Sec. III for the radiation patterns shown in Fig. 7. It can be readily seen that the agreement between theory and experiment is very good. Also, it is interesting to note that that the fractional mode content varies over a wide range (e.g., ~40 dB for the TE_{02} mode). Without higher order mode beam–wave interaction, one would expect the modal content for the TE_{02} and TE_{03} to remain constant at approximately −32.5 and −44.5 dB, respectively, of the total outgoing rf power.

In general, a lower input power results in greater modal impurities. This is because at low input power the beam is still very energetic upon entering the uptaper, resulting in stronger higher order mode interaction. Surprisingly, at extremely low input power, the TE_{03} mode can exceed the TE_{02} mode, and even exceed the TE_{01} operating mode at the lowest power, as can be seen in Fig. 12. This is also confirmed by experimental data at the 1/16th saturated power point (0.009 W of input power) where the TE_{03} power exceeds the TE_{02} power. An exception, however, is the fractional mode content of the TE_{02} mode at around the 1 W input power point. Here, the TE_{02} mode content dips as low as −46 dB of the total output power, well below the −32.5 dB of the cold case. This is because near this point, for the particular physical parameters employed, the electron beam becomes overbunched. This leads to rf power absorption rather than excitation for this particular mode (TE_{02}) and, consequently, the dip below the cold case.

Comparisons between theory (solid line) and experimental data (dots) for the fractional mode content for the TE_{02}, TE_{04}, and TE_{04}, across the frequency band at saturation (2.4 W drive power), are shown in Figs. 13(a)–13(c), respectively. The experimental data points correspond to the radiation patterns from Figs. 8(a) and 8(b). Again, the agreement between simulation and data is quite good. However, in contrast to Fig. 3, which shows relatively constant modal contents across the band in the beam's absence, the higher order mode fractions vary over a wide range in the presence of the electron beam. As expected from theory, the higher order mode contents are higher at the band edges than at the center, where the TE_{01} interaction is more efficient.

Experimental confirmation of the substantial variation of the mode contents versus frequency and output power level, as shown in this paper, strongly indicates that higher order mode excitation by the electron beam in the uptaper can indeed be a major source of perturbation to the rf power flow in nonlinear uptapers. This suggests that future taper designs may need to take into account the impact of this important effect in order to ascertain the modal purity of the taper design. While the examples discussed in this paper have focused on gyroklystron amplifiers, it should be emphasized that the effect is general and can also apply to any gyrodevices, including gyro-TWTs and oscillators.

V. CONCLUSIONS

In this paper, we have presented the theoretical basis and the experimental confirmation of the higher order mode excitation in gyro-device uptapers. It was shown that the presence of the electron beam could substantially modify the modal contents of the rf power. The presence of unwanted modes can adversely impact the performance of the ensuing transmission lines and creates unnecessary sidelobes in the radiation patterns. In the particular example presented here, the effect due to beam excitation can be as high as 20 dB in terms of mode contents relative to the cold case. This effect is most pronounced when the interaction with the operating mode in the main interaction circuit is weak, such as at the band edges or below saturation. However, since the interaction is that of a gyro-traveling-wave type and thus depends on the resonance condition, this suggests that the effect can be greatly reduced by carefully selecting the taper and magnetic field axial profiles so that the resonance length can be kept at a minimum. Moreover, minimizing the peak of the higher order modes of the taper internal conversion (see Figs. 1 and 2), which serves as the seed for the amplification, also can potentially result in a higher mode purity. The results presented in this paper strongly suggest the need to take into account the potential impact of beam–wave interaction in the design of gyro-device output tapers by employing self-consistent design codes, such as MAGY.

[1]K. T. Nguyen, B. G. Danly, B. Levush, M. Blank, R. True, G. R. Good, T. A. Hargreaves, K. Felch, and P. Borchard, IEEE Trans. Plasma Sci. **26**, 799 (1998).
[2]A. Mobius and M. Thumm, in *Gyrotron Oscillators: Their Principles and Practice*, edited by C. J. Edgecombe (Taylor and Francis, Bristol, PA, 1993), Chap. 7.
[3]W. G. Lawson, IEEE Trans. Microwave Theory Tech. **38**, 1617 (1990).
[4]M. Botton, T. M. Antonsen, Jr., B. Levush, K. T. Nguyen, and A. N. Vlasov, IEEE Trans. Plasma Sci. **26**, 882 (1998).
[5]K. T. Nguyen, B. Levush, T. M. Antonsen, Jr., M. Botton, M. Blank, J. P. Calame, and B. G. Danly, IEEE Trans. Plasma Sci. **28**, 867 (2000).
[6]M. Garven, J. P. Calame, K. T. Nguyen, B. G. Danly, B. Levush, and F. Wood, IEEE Trans. Plasma Sci. **28**, 672 (2000).
[7]J. P. Calame, M. Garven, J. J. Choi, K. Nguyen *et al.*, Phys. Plasmas **6**, 285 (1999).
[8]J. J. Choi, A. H. McCurdy, F. N. Wood, R. H. Kyser, J. P. Calame, K. T. Nguyen, B. G. Danly, T. M. Antonsen, Jr., B. Levush, and R. K. Parker, IEEE Trans. Plasma Sci. **26**, 416 (1998).
[9]M. Blank, B. G. Danly, B. Levush, J. P. Calame, K. Nguyen, D. Pershing, J. Petillo, T. A. Hargreaves, R. B. True, A. J. Theiss, G. R. Good, K. Felch, B. G. James, P. Borchard, P. Cahalan, T. S. Chu, H. Jory, W. G. Lawson, and T. M. Antonsen, Jr., Phys. Plasmas **6**, 4405 (1999).
[10]C. Balanis, *Antenna Theory* (Harper and Row, New York, 1982), Chap. 11, p. 446.
[11]K. T. Nguyen, J. P. Calame, B. G. Danly, B. Levush, M. Garven, and T. Antonsen, Jr., "Design of a *Ka*-band gyro-TWT for Radar Applications," IEEE Trans. Electron Device (in press).
[12]W. B. Herrmannsfeldt, SLAC, Stanford, CA, Report, No. 226, 1979.